ACS Biomaterials SCIENCE & ENGINEERING
Article
Cite This: ACS Biomater. Sci. Eng. XXXX, XXX, XXX−XXX

Calcium-Deficient Hydroxyapatite/Collagen/Platelet-Rich Plasma Scaffold with Controlled Release Function for Hard Tissue Regeneration

JiUn Lee and GeunHyung Kim*

Department of Biomechatronic Engineering, College of Biotechnology and Bioengineering, Sungkyunkwan University (SKKU), Suwon, Korea

Supporting Information

ABSTRACT: Calcium phosphate cement scaffolds have been extensively used in bone tissue regeneration applications because they are similar to the inorganic components of bones and have outstanding biocompatibility. However, the main shortcomings of ceramic scaffolds are their brittleness and low retention level of various growth factors or drugs. To overcome these shortcomings, we have reinforced ceramic scaffolds using synthetic and natural polymers as composites. Here, we designed a new bone-biomimetic composite consisting of calcium deficient hydroxyapatite (CDHA), collagen, and plate-rich plasma (PRP) using low temperature printing process. In the biocomposite, we manipulated the release of the bioactive component, PRP, which has several growth factors, for a long culture period (up to 35 days) by using a polyphenol, tannic acid. The mesh-structured biocomposite showed structural stability. We also tested the in vitro biocompatibilities of the biocomposite using preosteoblasts (MC3T3-E1) and found that the biocomposite showed better cell growth and differentiation compared to the control (fabricated without PRP). Although effects of platelet-rich plasma have remained controversial, our results indicated controlled release of PRP with a biocomposite showed enhanced proliferation and differentiation of preosteoblast cells.

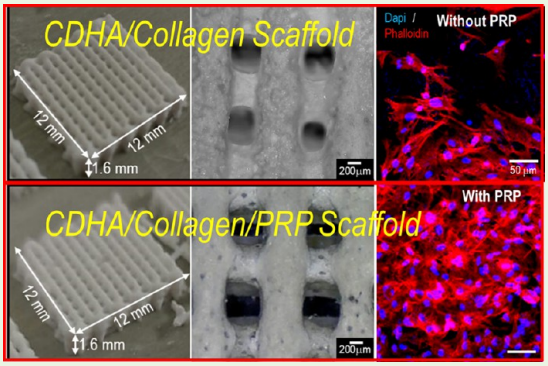

KEYWORDS: *low-temperature 3D printing, PRP release, tissue engineering, bone*

1. INTRODUCTION

Until now, bone regeneration in the human body has been one of the main issues of tissue engineering applications because of the increase in several musculoskeletal defects caused by tumors, diseases, traffic accidents, war, and even bone birth defects. It has been well-recognized that autografts can be the gold standard for bone grafts, because they have the desired properties of nonimmunogenicity and retain various important biocomponents such as bone morphogenic proteins and other growth factors, with a three-dimensional (3D) porous structure.[1] However, limited sources and a requirement for secondary operations have been major limitations in the use of autografts.[2] To overcome these problems, researchers have developed artificial bone grafts (scaffolds) as potential alternatives to autografts. Moreover, the combination of scaffolds and systemic drug delivery has been widely researched because proper drug delivery can directly accelerate the healing or the regeneration of bone tissues. However, uncontrolled drug delivery with scaffolds can evoke undesirable side effects;[3] therefore, a scaffold capable of systemic and efficient drug delivery without an initial burst effect is required.

Various osteogenic drugs and growth factors have been investigated because of their prospective usage in bone tissue regeneration.[4] Among these, platelet-rich plasma (PRP) has been widely used in the treatment of various soft and hard tissues such as nerves, tendons, ligaments, and bones, because it has pro-angiogenic properties and it induces endothelial cells to show a pro-osteogenic phenotype.[1,5] This phenomenon occurs due to the many growth factors and cytokines contained in PRP, such as transforming growth factor beta 1 (TGF-β1), platelet-derived growth factor (PDGF), vascular endothelial growth factor (VEGF), and insulin-like growth factor (IGF).[6,7]

Bioceramics and calcium phosphate cements (CPCs) have been widely used for various hard tissue regenerations due to their compositional similarity to bone minerals and good osteoconductivity.[8−10] Calcium-deficient hydroxyapatite (CDHA), a type of CPC, shows easier biodegradation and higher cellular activities compared to other hydroxyapatite.[9] CDHA can be obtained through the hydrolysis [3α-$Ca_3(PO_4)_2$(s) (α-TCP) + H_2O(g) → $Ca_9(HPO_4)(PO_4)_5(OH)$ (s) (CDHA)] of alpha-tricalcium phosphate (α-TCP), which increases the mechanical properties of the material.[11,12] To achieve improved biological activities, researchers have also investigated various CDHA/synthetic polymer composites

Received: August 31, 2017
Accepted: December 1, 2017
Published: December 1, 2017

© XXXX American Chemical Society

DOI: 10.1021/acsbiomaterials.7b00640
ACS Biomater. Sci. Eng. XXXX, XXX, XXX−XXX

combined with growth factors.[3,13,14] However, although drug-delivering scaffolds using synthetic polymers (such as poly-L-lactide and poly(ε-caprolactone)) can provide reasonable in vitro release performance of drugs, the use of these scaffolds is associated with some issues such as low levels of osteogenesis and toxic byproducts produced during scaffold degradation.[15] Therefore, ceramic-based scaffolds using a natural biomaterial (collagen) have been considered a good alternative due to their outstanding biological properties and nontoxicity.[16] Recently, a collagen/HA (a ratio of 1/2 (w/w)) composite scaffold was fabricated using a low-temperature (4 °C) 3D printing process to regenerate bone tissues, and the scaffold was found to induce significantly high cell adhesion, proliferation, and even osteogenic differentiation of bone marrow stromal cells.[8] However, the authors failed to show the capability of the ceramic-based scaffold for drug release; this scaffold also had poor mechanical properties. The fabrication of a bioceramic scaffold constituted with a high volume percent (over 70 vol %) of ceramics and embedded with various osteogenic growth factors and having a precisely manipulated pore structure using conventional 3D printing is difficult, because it requires a reasonable volume percent of binder and post harsh-treatments to support its complex structure.[17] To overcome this challenging issue, in this study, we chose α-TCP/collagen (80% (v/v)) as an ink, because α-TCP can transform phase into CDHA at aqueous solution at low temperature (<40 °C),[12] which did not cause denaturation of collagen.[18] Tannic acid (TA), which is a nontoxic polyphenolic material, was used as a collagen-cross-linking agent and growth-factor-delaying component. Thus, we fabricated the α-TCP/collagen scaffolds using two different 3D printing processes: low-temperature printing (LTP, printing temperature: −16 °C to −18 °C) and room-temperature printing (RTP, printing temperature: 38 to 40 °C). By evaluating the printability of the α-TCP/collagen, a processing window for achieving a stable porous ceramic structure was selected. On the basis of the processing condition, we fabricated α-TCP/collagen/platelet-rich plasma scaffolds. The fabricated scaffolds were done proper postprocess (tannic acid cross-linking and hydrolysis) to make the transformation phase of α-TCP to CDHA and controlled release of PRP. The release of the growth factors (TGF-β1 and PDGF) in the PRP from the mesh-structured biocomposite were then examined and various in vitro cellular aspects such as cell viability, DAPI/phalloidin staining, and mineralization were evaluated to observe the effect of the PRP release behavior on bone tissue regeneration.

2. EXPERIMENTAL SECTION

Materials. Preosteoblasts (MC3T3-E1; ATCC, Manassas, VA, USA) were used for the in vitro experiments. Lyophilized type-I collagen from porcine skin (Aptgen, Seoul, South Korea) was used for scaffold fabrication, and TA (0.05−0.5 wt %; Sigma-Aldrich, St. Louis. MO, USA) in phosphate-buffered saline (PBS) was used as the cross-linking reagent. Bovine serum albumin (BSA) was used as a model protein to evaluate growth factor release. α-TCP (particle sizes: 4.57 ± 2.07 μm) was kindly provided by Dr. H.-S. Yun (Powder and Ceramics Division, Korea Institute of Materials Science, Changwon, South Korea). PRP extracted from guinea pigs was kindly provided by Prof. ChulHo Jang (Chonam National University Medical School, Gwangju, South Korea).

Preparation of Platelet-Rich Plasma (PRP). Platelet-rich plasma was prepared followed a method reported by Kim et al.[19] Briefly, 10 mL of blood extracted from guinea pig was mixed with 1 mL of anticoagulant solution (3.8% sodium citrate). The mixture centrifuged in centrifugation apparatus (Placon, Oscotec, South Korea) for 3 min at 2000g to separate red blood cells. A second centrifugation was performed for 5 min at 5000g to get the upper layer and buffer coat layer. Subsequently, PRP was obtained by suspending the remaining layer. The PRP was prepared as a gel by mixing with 1:1 mixture of 10% thrombin and 10% calcium gluconate. According to Ohtori et al., lyophilized PRP maintains growth factor expression compared with room-temperature preserved PRP.[20] Therefore, PRP freeze-dried for long period preservation, and 1 mg of PRP was dissolved in 1 mL of phosphate buffered saline (PBS) before use.

Fabrication of the Scaffolds. Collagen (4 wt %), α-TCP (80% (v/v)), and PRP (1 mg/mL) were mixed together and the volume fraction was calculated using the density of each material (collagen: 1.343 g/cm,[21] α-TCP: 2.866 g/cm[11]). A three-axis robot (DTR-3−3310-T-SG, DASA Robot, South Korea) and a dispensing system (AD-3000C, Ugin-tech, South Korea) were used to obtain a multilayered mesh structure (Figure 1a). A low-temperature printing system was used for the fabrication of the 3D mesh scaffold (working stage temperature: −16 °C to −18 °C; Figure 1b). Next, the fabricated scaffolds were lyophilized in a freeze-dryer (FD8505, IlshinBioBase, South Korea) for 12 h, followed by immersion in TA solution (0.1 wt % in PBS) for 10 min for collagen cross-linking. After rinsing with distilled water (DW) twice, the scaffolds were immersed in PBS for 24 h to hydrolyze α-TCP, lyophilized for 12 h, and then stored at −80 °C in a deep freezer until use (Figure 1(c)).

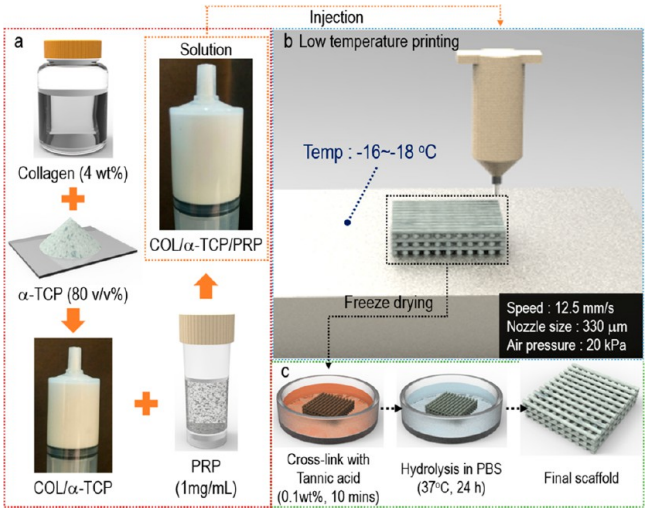

Figure 1. Schematics of (a) collagen mixture preparation, (b) low-temperature printing system (LTP), and (c) cross-linking with tannic acid and hydrolysis of α-TCP in PBS.

Rheological Testing. The rheological property (storage modulus (G')) of the collagen/α-TCP (80% (v/v)) solution was evaluated using a rotational rheometer (Bohlin Gemini HR Nano; Malvern Instruments, Surrey, UK) installed with cone-and-plate geometry (40 mm diameter, 4° cone angle, 150 μm gap). Temperature translation (from 15 to 50 °C) was conducted with 1% strain and 1 Hz frequency. Temperature and strain were set to 37 °C and 1% respectively for frequency sweep tests (0.1 Hz ∼ 10 Hz). The α-TCP/collagen solution stored at ordinary temperature until the tested started.

Characterization of the Fabricated Scaffolds. Thermogravimetric analysis (TGA) was performed using Exstar 6000 (Seiko Instruments, Chiba, Japan). Temperature translation (from 20 to 800 °C) was conducted at a uniform heating rate of 20 °C/min for 3 mg of the samples. The phase composition of the lyophilized samples was measured using X-ray diffraction (XRD, X'Pert PRO MPD, PANalytical, Netherlands) at an operating voltage of 40 kV and value of 2θ angle (range: 10−50°). On the basis of the XRD data, we calculated the crystallite size using the Scherrer equation $d = 0.9\lambda/\beta\cos\theta$, where d is the crystallite size, λ is the wavelength of the X-radiation, β is the full width at half-maximum (fwhm), and θ is the Bragg angle.[22]

DOI: 10.1021/acsbiomaterials.7b00640
ACS Biomater. Sci. Eng. XXXX, XXX, XXX−XXX

The surface morphology of the samples was evaluated using an optical microscope (DIMIS-M, Siwon Optical Technology, South Korea) and scanning electron microscope (SEM; SNE-3000M, SEC Inc., South Korea). Based on the SEM images, the dimension of the scaffold strut was calculated using ImageJ software (National Institutes of Health, Bethesda, MD, USA).

The porosity (%) of the scaffolds was calculated using the eq $[1 - (M\mathrm{WF}_{\mathrm{col}}/\rho_{\mathrm{collagen}} + M\mathrm{WF}_{\mathrm{TCP}}/\rho_{\mathrm{TCP}})/V_{\mathrm{total}}]100$, where M is the total weight, ρ is the density, V_{total} is the volume of the structure (assumed cubic), and $\mathrm{WF}_{\mathrm{col}}$ and $\mathrm{WF}_{\mathrm{TCP}}$ are the collagen and α-TCP weight fractions, respectively.

The mechanical property of the dried samples was measured in compressive mode using a universal testing instrument (Top-tech 2000; Chemilab, South Korea) at room temperature. Stress−strain curves were evaluated at a compression rate of 0.2 mm/s with cubic shape of 5 × 5 × 1.5 mm size. Hydrophilicity was indirectly measured by dropping 5 μL of α-MEM on the scaffolds for checking the contact angle.

The fabricated scaffolds were immersed in 10 U/mL collagenase (ThermoFisher Scientific, USA) solution to evaluate the degradation rate. The test was performed at 37 °C until 14 days, and the collagenase solution changed every day. At specific time point, the scaffolds were washed with distilled water and weighed after lyophilization (W_t). Degradation rate was calculated with the following equation: degradation rate (%) = $(W_I - W_t)/W_i100$, where W_i is weight of before degradation.

Analysis of Model Protein Release. To evaluate protein release characteristic by tannic acid, we chose bovine serum albumin (BSA) cas a model protein for release experiment because of its characteristics and acceptance.[23,24] Collagen solution (4 wt %) mixed with BSA (0.1 mg/mL) and lyophilized to fabricate cylinder collagen spongy scaffold. The collagen spongy contained BSA was immersed in 0, 0.05, 0.1, 0.25 wt % tannic acid solution for 10 min. The final scaffolds were placed into 500 μL of PBS at 37 °C. The supernatants around the samples were extracted and replaced with 500 μL of PBS at 1, 3, 7, and 10 days. Cumulative release of BSA from each scaffold was evaluated using the fluorescamine assay (Sigma-Aldrich, St Louis, MO, USA).[25] Briefly, 3 mg/mL fluorescamine solution was dissolved in acetone, and 150 μL each of the sample and control solutions were added along with 50 μL of fluorescamine solution. Fluorescence quantification was measured at an excitation wavelength of 395 nm and an emission wavelength of 475 nm using a microplate reader (Synergy H1 Hybrid Reader; BioTek Instruments). Protein concentration was calculated from the standard curve of the quantified fluorescence.

Analysis of the Release Behavior for PRP-Derived Growth Factors (TGF-β1 and PDGF). The fabricated biocomposites were immersed in 2 mL of α-minimum essential medium (α-MEM; Gibco) at 37 °C. The release of TGF-β1 and PDGF was measured after the hydrolysis reaction in PBS for 24 h for total loss. Then, the release was measured at 12 h and 1, 3, 5, 7, 10, 14, 21, 28, and 35 days. At each time point, 1 mL of the medium were extracted around each sample and replaced with 1 mL of new medium. The collected medium was stored in 1.5 mL tubes at −80 °C until all the samples were collected. The concentrations of guinea pig TGF-β1 and PDGF were determined using commercially available enzyme-linked immunosorbent assay (ELISA) kits (Genorise Scientific, USA). All the TGF- β1 and PDGF samples were diluted at 1:200 and 1:100 ratios, respectively. The immunoassays were performed according to the manufacturer's instructions.

Preosteoblast (MC3T3-E1) seeding on the scaffolds. The activities of the MC3T3-E1 cells were evaluated with the fabricated scaffolds (5 × 5 × 1.5 mm). The cells were cultured in α-MEM (Gibco) supplemented with 10% fetal bovine serum (FBS; Gemini Bio-Products) and 1% penicillin-streptomycin (HyClone). The cells were collected by treatment with trypsin-EDTA (ethylenediaminetetraacetic acid) solution and counted with hemocytometer (Marienfeld-Superior, Germany). The counted cells were resuspended with α-MEM (1.0×10^7 cells/mL), and 20 μL of medium (2.0×10^5 cells) pipet onto the surface of the scaffolds. After 4 h incubation, 400 μL of medium added each sample. They were then placed in an incubator (MCO-20AIC, SANYO Electric, Japan) under 5% CO_2 at 37 °C. The medium was changed every 2 days.

Cell-seeding efficiency was measured using the method of Sobral et al.[26] Briefly, for cell attachment, the cells were allowed to remain on the scaffolds for 12 h, after which the scaffolds were taken out, and the cells remaining in the wells were counted. On the basis of the number of cells remaining in the well (n_{well}) and the initial number of cells (n_{ini}), the seeding efficiency of each scaffold was calculated using the following equation: seeding efficiency (%) = $(n_{\mathrm{ini}} - n_{\mathrm{well}})/(\mathrm{n}_{\mathrm{ini}}) \times 100$.[26]

Live/Dead Cell Assay and Cell Proliferation Analysis. The scaffolds were exposed to 2 mM calcein AM and 2 mM ethidium homodimer-1 for 45 min in an incubator for cell viability evaluation. A microscope (TE2000-s, Nikon, Japan) equipped with epifluorescence attachment and a SPOT RT digital camera (SPOT Imaging Solutions, Sterling Heights, USA) was used to analyze the stained cells on the scaffolds. The images were randomly captured in four different area of each scaffolds. Cell viability was evaluated by the capturing images at 4 h and at 1, 3, 6, and 9 days, and the number of live (green) and dead (red) cells were counted using the ImageJ software (National Institutes of Health). Cell viability was calculated as the ratio of the live cells to the total number of cells.

The PicoGreen assay was used to measure cell proliferation. The samples were washed with PBS twice and transferred to 1.5 mL tubes at 4 h (initial) and 1, 3, 6, and 9 days. Then, 1 mL of cell lysis buffer (10 mM Tris pH 8, 1 mM EDTA, and 0.2% (v/v) Triton X-100) was added to each sample for 30 min. The samples were then mixed using a vortex (Vortex-Genie 2, Scientific Industries, Inc. NY, USA) for 10 s every 5 min. The cell lysate was then frozen at −80 °C until all the samples were collected; then, each sample was thawed at the same time for measurement of the dsDNA concentration. A Quant-iT PicoGreen dsDNA kit (Molecular Probes) was used according to the manufacturer's protocol. Briefly, the Quanti-iT PicoGreen reagent was diluted to 1:200 with trypsin-EDTA (ethylenediaminetetraacetic acid) buffer. The prepared reagent was then mixed with the sample solution at a 1:1 ratio. The sample fluorescence was measured using a microplate reader (Synergy H1 Hybrid Reader; BioTek Instruments) with excitation at 480 nm and emission at 520 nm. The standard curve was drawn according to the manufacturer's protocol.

DAPI/Phalloidin Staining and Analysis. The nuclei and F-actin of the cells on the scaffolds were stained with diamidino-2-phenylindole (DAPI; dilution ratio of 1:100, Invitrogen, Carlsbad, CA, USA) and Alexa Fluor 568 phalloidin (dilution ratio of 1:100, Invitrogen) at 6, 9, and 12 days. The stained samples were then visualized using a confocal laser scanning microscope (LSM-700, Zeiss, Germany). Four randomly captured images were used to measure the nuclei density and F-actin area using the ImageJ software (National Institutes of Health).

Analysis of Osteogenic Activities. Alkaline phosphatase activity of the MC3T3-E1 cells on the scaffolds was evaluated using the Alkaline Phosphatase Yellow (pNPP) Liquid Substrate System for ELISA (Sigma Life Science, USA). The scaffolds with the cells were washed with PBS twice, and 200 μL of pNPP solution was added to them. After incubation for 2 h, 50 μL of 3 N NaOH solution was added to each sample to stop the reaction. Each sample was then analyzed using a microplate reader (EL800, BioTek, USA) by measuring the absorbance at 405 nm.

The optical extent of calcium mineralization of the scaffolds with the cells was analyzed using Alizarin Red S staining. The scaffolds were washed twice with PBS and fixed in 70% (v/v) ice ethanol (4 °C) for 30 min. The fixed scaffolds were then stained with 0.04 mM Alizarin Red S (pH 4.2) for 1 h, followed by washing with DW until the red dye was completely released. Each scaffold was then lyophilized and captured randomly using an optical microscope. The optical images were analyzed with image J software to evaluate the degree of calcium deposition using red color intensity.

For immunofluorescence staining of osteopontin (OPN), we proceeded with the protocol proposed by Park et al.[27] Briefly, the cells on the scaffolds were fixed with 3.8% (w/v) paraformaldehyde (Sigma-Aldrich, St. Louis, MO, USA) in PBS for 10 min at room temperature. Next, 0.1% (v/v) Triton-X 100 (Sigma-Aldrich, St. Louis, MO, USA) in PBS was added to the scaffolds for 5 min, and the cells were washed three times with PBS. The cells were then incubated with 1% (v/v) BSA in PBS for 30 min at room temperature to prevent nonspecific binding of the antibodies. Next, after washing three times

DOI: 10.1021/acsbiomaterials.7b00640
ACS Biomater. Sci. Eng. XXXX, XXX, XXX−XXX

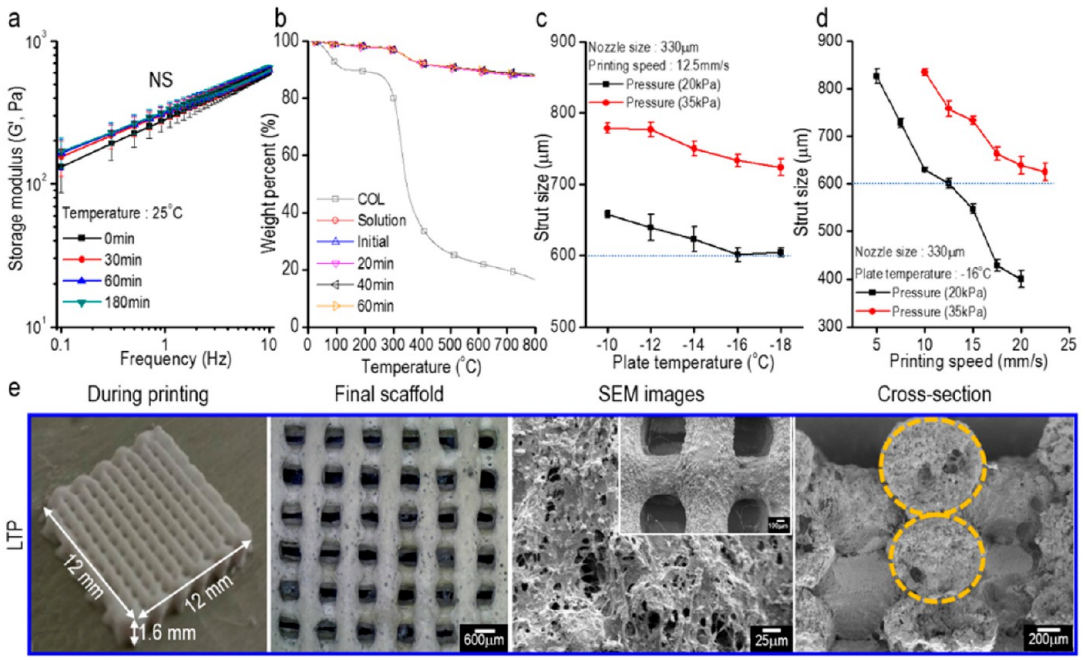

Figure 2. (a) Rheology data of collagen/α-TCP solution with different storage time (0, 30, 60, 180 min) at 25 °C. (b) Results of TGA of pure collagen and collagen/α-TCP structures fabricated at different interval times (in situ, 20, 40, and 60 min). Strut size analysis of the printed scaffolds at different (c) working stage temperatures and (d) printing speeds. (e) Optical and SEM images of the biocomposite fabricated using LTP. NS means not significant.

with PBS, the scaffolds were incubated with primary antibodies (antiosteopontin antibodies, Abcam, Cambridge, UK) at 4 °C overnight. The cells were then washed three times with PBS for 5 min each and treated with Alexa Fluor 488-conjugated goat antimouse secondary antibodies (1:100; Invitrogen, Carlsbad, CA, USA) in PBS, followed by incubation for 1 h at room temperature before the fluorescence images were taken using the confocal laser scanning microscope.

Statistical Analysis. All the data are represented as means ± standard deviation (SD), and each experiment was conducted in at least three ($n \geq 3$). Two different types of statistical analysis were done with the SPSS software (ver. 20.0, SPSS, Inc., Chicago, IL, USA); One is student's t test for two groups analysis, and the other is one-way analysis of variance (ANOVA) for more than three groups. In all the analyses, $p < 0.05$ was considered to indicate statistical significance (*).

3. RESULTS AND DISCUSSION

3.1. Evaluation of α-TCP/Collagen Paste and Printing Conditions To Attain a Stable Structure of the Ceramic-Based Biocomposite. It is known that α-TCP transforms to calcium deficient hydroxyapatite (CDHA) in aqueous solution.[12] This can cause early hydrolysis of α-TCP before the printing process. Therefore, we evaluated the storage modulus of the printing solution prepared with α-TCP (80v/v%) and collagen (4 wt %). According to Kalyon et al., the storage modulus significantly increased as calcium phosphate ceramic changed to calcium phosphate cement.[28] In this study, the storage modulus of α-TCP/collagen solution was measured at different time intervals (0, 30, 60, 180 min) immediately after preparing the solution (Figure 2a). The rheological data showed that there was no significant difference in α-TCP/collagen solution until 180 min stored at 25 °C. The nucleation period and completion time for hydrolysis extends as the temperature decreases.[12] On the basis of this result, we confirmed that the solution can be used or stored until 180 min at 25 °C without significant difference in the α-TCP phase transformation.

When printing with a mixture consisting of organic and inorganic components with highly different densities, one of the main problems faced during the extrusion printing process can be the time-dependent homogeneity of the components for the printed struts caused due to the sedimentation of high-density materials in the extruding barrel. In our case, α-TCP has higher density (2.866 g/cm^3) than collagen (1.343 g/cm^3), which made it necessary to consider the time-dependent sedimentation of the bioceramic in the printing barrel. To measure the homogeneity of the fabricated strut for various time periods, the mesh structures, all of which have the same pore structure, were fabricated with four time intervals (in situ, 20, 40, and 60 min) after injecting the mixture into the barrel. The α-TCP weight fraction of the fabricated structures was then evaluated using the results of TGA (Figure 2b). Until 60 min, the weight fraction (87 ± 0.2%) of α-TCP in the biocomposites was the same. On the basis of this result, we fabricated all mesh structures within 60 min after injecting the mixture into the barrel.

In this work, we fabricated ceramic-based biocomposites using two different processes: LTP and RTP (room temperature printing, printing temperature: 38 to 40 °C) (Figure 1b, Figure S1a). We chose LTP process considering internal pore structure, and printability. As shown in Figure 1b, the LTP process uses a low-temperature working plate (−16 °C) to freeze the extruded struts. A single line test was conducted to select an appropriate printing condition. In general, the working stage temperature, pneumatic pressure, and printing speed are known to be critical processing parameters. In this study, we used two different pneumatic pressures (20 and 35 kPa), and the nozzle size (330 μm) was fixed. Figure 2c shows the effect of the temperature of the working stage on the strut diameter. The mixture of collagen and α-TCP froze immediately when the mixture was contacted on the cooled working stage. However, the composite struts that were processed at a temperature above −16 °C were larger and unstable because of the insufficient quenching of the strut. In addition, the effect of the moving speed on the strut diameter was

DOI: 10.1021/acsbiomaterials.7b00640
ACS Biomater. Sci. Eng. XXXX, XXX, XXX−XXX

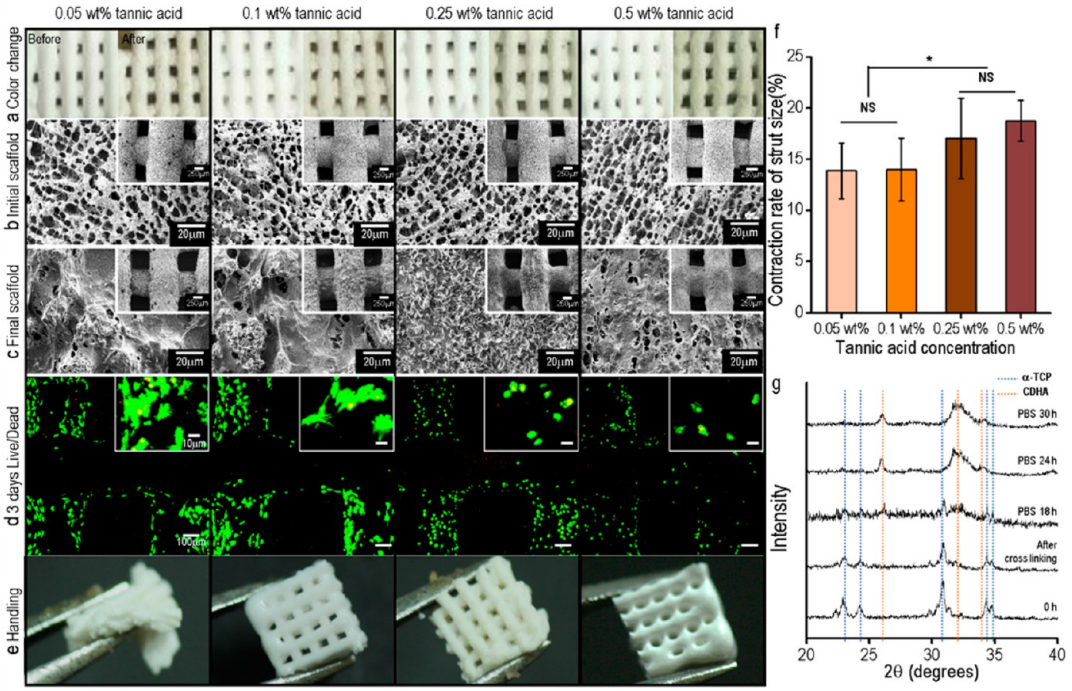

Figure 3. (a) Optical color change of scaffolds before and after cross-linking with different TA concentrations (0.05, 0.1, 0.25, and 0.5 wt %). Surface morphology of the printed struts of (b) in situ fabricated biocomposite and (c) biocomposites cross-linked using various concentrations of TA. (d) Live (green)/dead (red) images of MC3T3-E1 cell-seeded scaffold after 3 days. (e) Sample handling. (f) Comparison of the biocomposite contraction for the TA concentration. (g) XRD results of the fabricated biocomposites in PBS (37 °C) at various time intervals (0 h, just after cross-linking, 18, 24, and 30 h). * indicates $p < 0.05$, and NS means not significant.

evaluated (Figure 2d). As expected, the strut diameter linearly decreased with an increase in the moving speed. Based on this result, to obtain the strut size of 600 μm, we used the following processing conditions for the LTP process: temperature of the working plate, −16 °C; moving speed, 12.5 mm/s; and pneumatic pressure, 20 kPa.

Thus, we successfully fabricated the mesh structures of the biocomposite using the LTP with the dimension of 12 × 12 × 1.6 mm (3 layers). The scaffolds in Figure 2e show the surface and cross-sectional optical and SEM images of the structures. As shown in the images, the structure was designed with 3D pore geometry (pore size, 400 ± 18.3 μm; and strut size, 601 ± 17.7 μm).

3.2. Cross-Linking of Collagen in the Biocomposite Using TA. After printing the mesh structure using the LTP process, the biocomposite was cross-linked using TA. To observe the toxicity of TA toward cells, after cross-linking the biocomposites with various concentrations (0.05−0.5 wt % in PBS) of TA for 10 min, the cells (MC3T3-E1, 1 × 10^6 cells mL^{-1}) were cultured for 3 days. Figure 3a−d shows the optical, SEM, and the live/dead cultured cell images for 0.05, 0.1, 0.25, and 0.5 wt % of TA. As shown in the images, the fabricated structure remained stable for all TA concentrations and the porous structure on the printed struts was well sustained. Furthermore, as shown in the live/dead cell images, the viability of the cells was significantly high for all mesh structures, but the cells did not proliferate for the mesh structures cross-linked with more than 0.25 wt % of TA because high concentrations of TA caused cell fixation.[29] However, with regard to sample handing, the mesh structure cross-linked with 0.05 wt % of TA was too fragile compared to the other mesh structures (Figure 3e).

It has been well-known that the size stability is an important design factor for scaffold fabrication because a pore structure (pore size and porosity) that is optimal for various cell types cannot be obtained. Here, to observe the size stability of the biocomposite before and after the cross-linking, the percentage size reduction was calculated for various weight fractions of TA using the following formula: [total area of the biocomposite before cross-linking] - [total area of the biocomposite after cross-linking])/(total area of the biocomposite before cross-linking) × 100 (Figure 3f). The results showed that the size reduction of the biocomposite increased with an increase in the weight fraction of the cross-linking agent due to the contraction of the cross-linked collagen region. Based on our analyses of the live/dead cell images, physical handing, and percentage size reduction, we selected 0.1 wt % TA and a cross-linking duration of 10 min as optimum for cross-linking the collagen component in the biocomposites.

Figure 3g shows the XRD data for the mesh structure cross-linked with 0.1 wt % of TA before and after the hydrolysis reaction in PBS solution for various time periods until 30 h. As shown in the XRD data, the mesh structure before the cementation displayed the characteristic XRD peaks of α-TCP, which was due to its orthorhombic crystal structure. However, the hydrolysis of α-TCP after immersion of the mesh structure increased with an increase in cementation time until 24 h. Ultimately, the α-TCP was entirely converted to calcium-deficient hydroxyapatite (CDHA), which has a crystal structure corresponding to that of the inorganic ingredients in bones.[30] On the basis of this result, after cross-linking the biocomposite with TA, we immersed the biocomposite for 24 h to obtain the CDHA component in the biocomposite.

3.3. Fabrication and Characterizations of the Control and PRP Biocomposites. It is well-known that pore structure, including strut and pore size and porosity, is one of the important design factors in scaffold fabrication because it effects various

DOI: 10.1021/acsbiomaterials.7b00640
ACS Biomater. Sci. Eng. XXXX, XXX, XXX−XXX

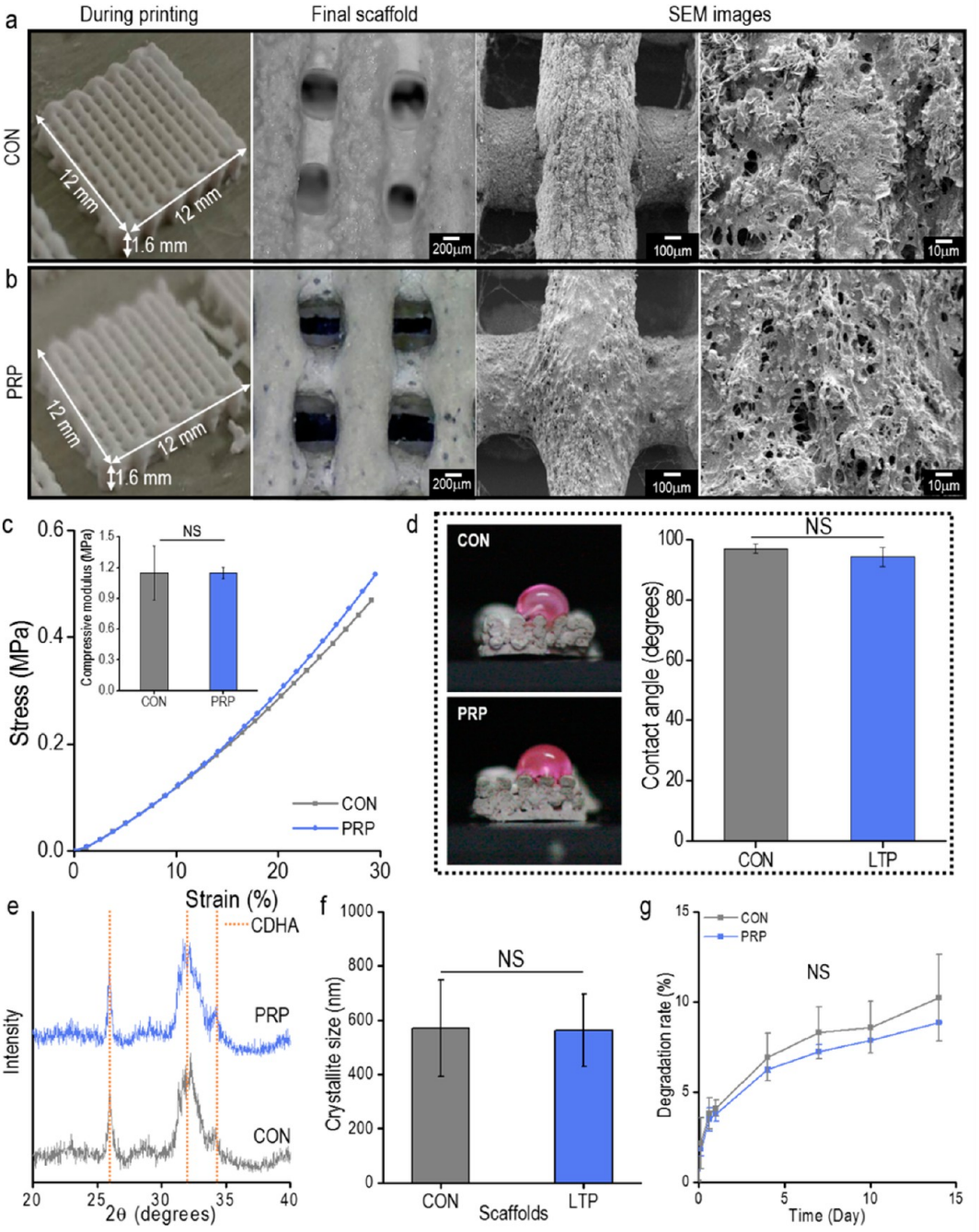

Figure 4. Optical and SEM images showing macro/micro morphology of (a) control (CON) and (b) PRP biocomposite (PRP). (c) Compressive stress−strain curve and inset figure showing the compressive modulus, (d) optical images showing water contact angle and the measured contact angle of the CON and PRP scaffolds. (e) XRD analysis, and (f) crystallite size based on the XRD data. (g) Degradation rate with collagenase solution of CON and PRP scaffolds. NS means not significant.

cellular responses to the scaffolds. However, high porosity causes decrease of scaffold mechanical properties, which is also an important factor for stability of scaffold.[31,32] So, it is important to optimize strut and pore size for achieving both mechanical properties (structure stability) and proper porosity (cellular activities). Recently, Lin et al. showed that the appropriate pore size and strut size of a collagen/hydroxyapatite scaffold were 400 and 600 μm, respectively, for regenerating bone tissues.[8] Therefore, we set this pore size and strut size for the biocomposite in our study. To determine the efficiency of the PRP in the biocomposite, we fabricated a control biocomposite consisted with collagen and CDHA without the PRP component using the low temperature 3D printing system, cross-linking, and hydrolysis process (Figure 4a). Figure 4b shows the biocomposite composed of collagen, CDHA, and PRP (PRP biocomposite) using the same fabrication method. As shown in the optical and SEM images, both biocomposites showed slightly roughened surfaces and well-fabricated macropores. In addition, the porosity of the composites was not significantly different (control, 83.69 ± 1.75%; and PRP biocomposite, 82.90 ± 0.60%).

DOI: 10.1021/acsbiomaterials.7b00640
ACS Biomater. Sci. Eng. XXXX, XXX, XXX−XXX

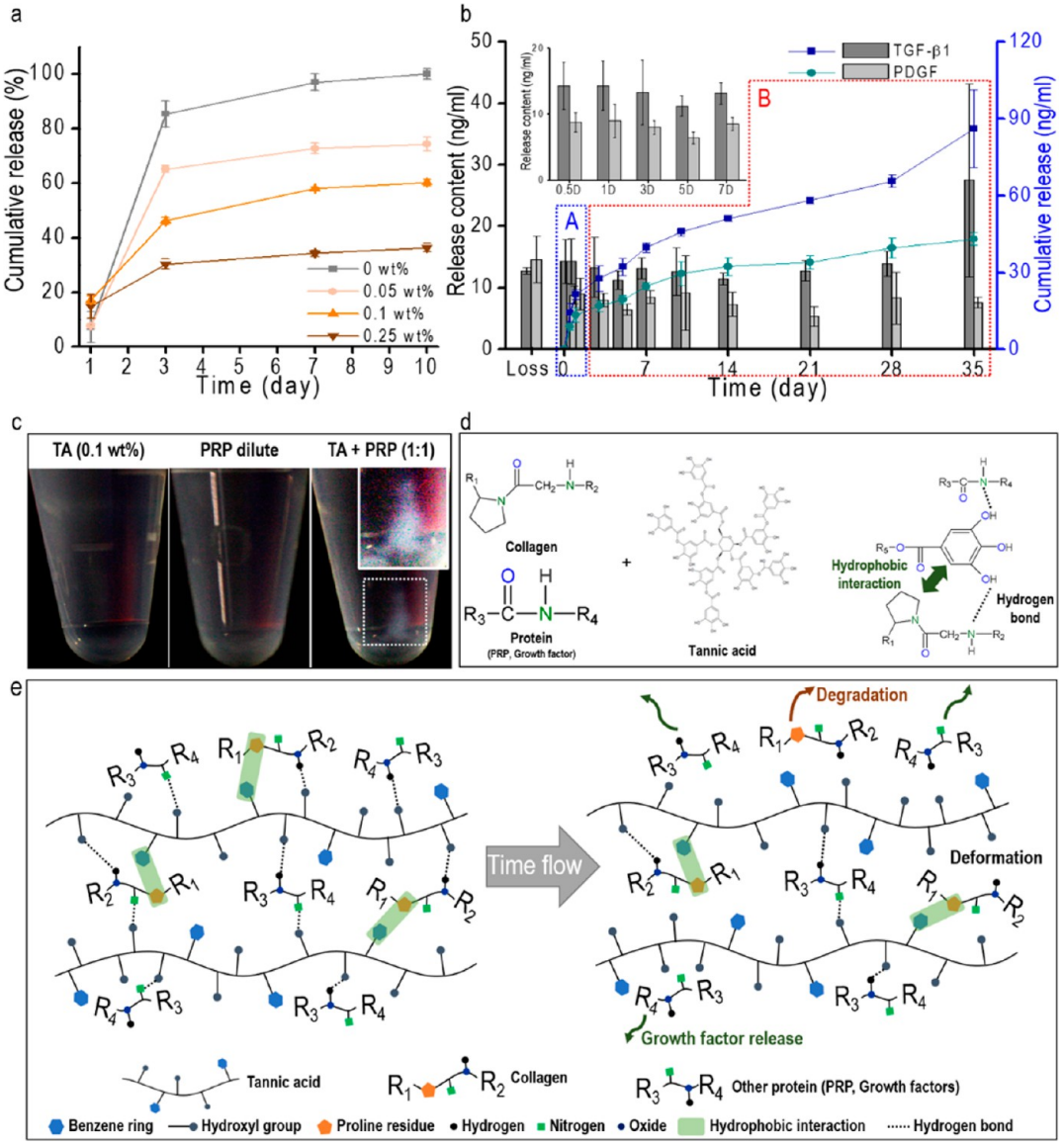

Figure 5. (a) Cumulative release of bovine serum albumin (BSA) from the collagen/BSA scaffolds cross-linked with tannic acid solutions of different concentrations (0, 0.05, 0.1, 0.25 wt %). (b) Amounts of TGF-β1 and PDGF released from the biocomposite scaffolds during 35 days. (c) Optical images of platelet-rich plasma (PRP) cross-linked with tannic acid. Schematics of (d) tannic acid cross-linking reaction between collagen and protein and (e) collagen degradation and growth factor release process.

Various physical properties of both the fabricated biocomposites were also characterized. The mechanical property of biomedical scaffolds is an important factor, because the cells can feel the mechanical stiffness of the scaffold, affecting cell proliferation and differentiation.[33] Figure 4c shows the compressive stress−strain curves and moduli of the control and PRP biocomposites; as expected, the calculated modulus was not significantly different between the two scaffolds (control, 1.15 ± 0.26 MPa; and PRP biocomposite, 1.15 ± 0.05 MPa).

Furthermore, surface wettability can also influence initial cell adhesion and proliferation.[34] Figure 4d shows the optical images of the contact angle of each scaffold; there was no significant difference between the two groups (control, 96.9 ± 1.47°; and PRP biocomposite, 94.2 ± 3.23°).

To observe the hydrolysis of the α-TCP component to CDHA in the biocomposites, we evaluated the XRD data (Figure 4e, f). The XRD crystal patterns showed that the hydrolysis of α-TCP to CDHA was well-achieved in both scaffolds. In addition, the crystallite size was calculated using the fwhm of the crystal peaks (2θ = 26, 31, 34°) and a Scherrer equation, $d = 0.9\lambda/\beta\cos\theta$, where d, λ, β, and θ are the crystallite size, X-ray wavelength (1.54 Å), fwhm, and Bragg angle, respectively. The crystallite size (d) of the control and PRP biocomposites was the same (573.5 ± 143.4 nm).

To evaluate the degradation rate of the fabricated scaffolds, we immersed the biocomposite into the collagenase solution. Figure 4g shows the results of degradation rate (CON: 10.22 ± 2.41%, and PRP: 8.85 ± 0.05%, and there is no significant difference between degradation rate of control and PRP scaffolds until 14 days.

Thus, we fabricated two collagen/CDHA-based biocomposites: a control biocomposite without PRP and an experimental biocomposite with the PRP component (PRP biocomposite). The results of the characterizations of the structures showed that both the biocomposites showed the same pore geometry and

DOI: 10.1021/acsbiomaterials.7b00640
ACS Biomater. Sci. Eng. XXXX, XXX, XXX−XXX

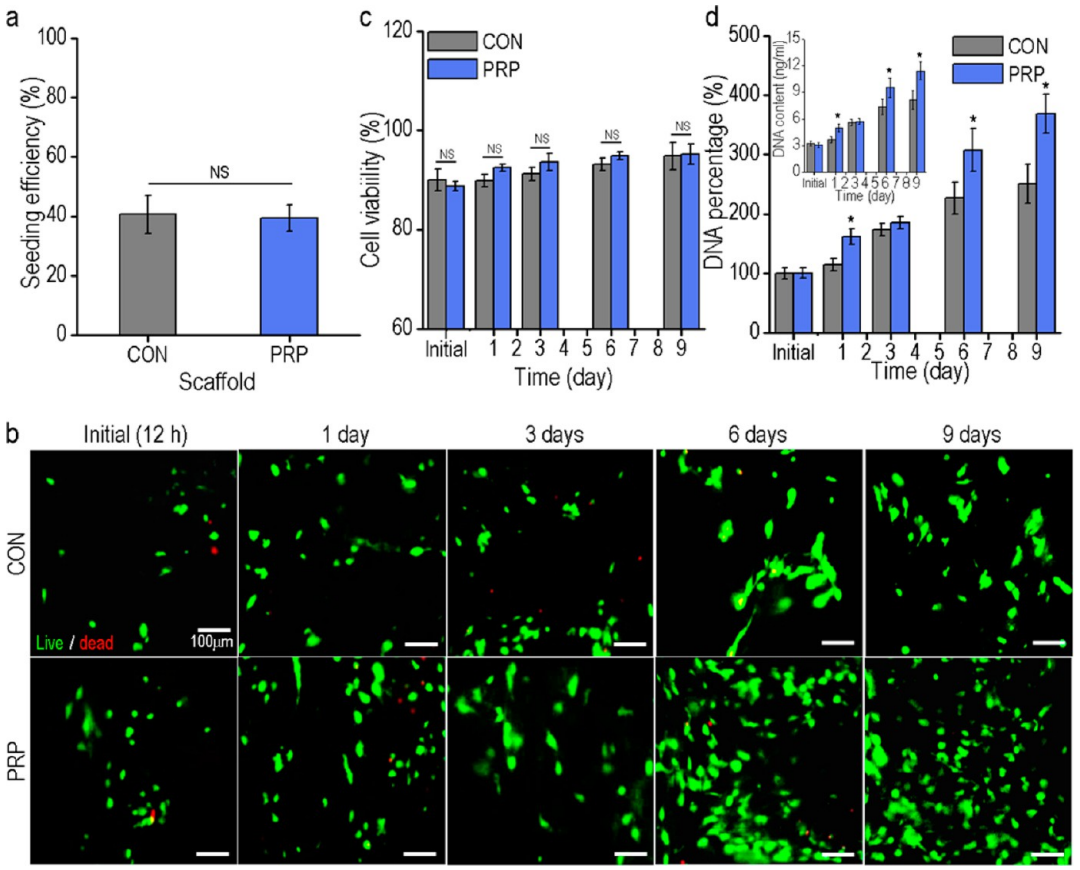

Figure 6. (a) Seeding efficiency of the CON and PRP scaffolds. (b) Live (green) and dead (red) images at 12 h, 1 day, 3 days, 6 days, and 9 days. (c) Cell viability and (d) PicoGreen assay results for the CON and PRP scaffolds for various culture periods. * indicates $p < 0.05$, and NS means not significant.

similar compressive modulus, wettability, crystal structure, and degradation rate.

Conventionally, collagen/TCP scaffolds prepared by mold or coating process,[35,36] and these scaffolds did not have fully interconnected pore structure. On the other hand, 3D printed collagen-based ceramic scaffolds have proper pore structure, but it showed very poor mechanical properties due to the absence of sintering process.[8,37] However, we successfully fabricated fully interconnected CDHA/collagen scaffolds, which showed comparatively better mechanical property by hydrolysis reaction.

3.4. PRP Release from the Biocomposites. PRP has been widely used in tissue regeneration as it contains various growth factors (TGF-β1, PDGF, IGF, VEGF, etc.),[38,39] and is also used in bone regeneration.[7,40−42] Especially, controlled release of PRP using alginate capsules showed enhancement both of proliferation and differentiation of human osteoblast like cells.[7] However, the controllability of the release of PRP-derived growth factors is still a challenge. Recently, thrombin-conjugated PRP was used to regenerate bone tissues, but the initial release of PRP-derived growth factors from the PRP-thrombin clot was about 90% within 24 h.[43] However, gelatin hydrogel showed more accurate controlled release of PRP-derived growth factors with enhanced bone regeneration compared to that of thrombin-PRP hydrogel.[44]

Tannic acid (TA) is a water-soluble natural polyphenolic material, and it is well-known that TA can cross-link proteins by forming hydrogen bond between hydroxyl groups of TA and peptide bonds of the proteins.[45] Due to this chemical properties, TA is used for cross-linking[46,47] collagen or gelatin and cell fixation.[29] We envisioned that this property could be used to control the release of growth factors. To observe the effect of various weight fractions of TA on the protein release, we used bovine serum albumin (BSA) as a model protein for drug-release indicator.[23] Figure 5a shows the release of BSA from the pure collagen (4 wt %) spongy. In the collagen without TA, a significant initial burst effect was observed; however, an increase in TA concentration in the collagen deterred the release of BSA. Moreover, the initial burst from the collagen cross-linked with TA was significantly decreased. This result indicated that TA could be used for delayed release of growth factors with increasing TA weight fraction. However, as we mentioned before, high concentration of TA occur cell fixation,[29] so we found the proper condition (0.1 wt % TA, for 10 min immersion) for TA cross-linking on the fabricated biocomposite (Figure 3a−e).

To evaluate whether this impediment of model protein release could be adapted to PRP, we investigated cumulative release of PRP-derived growth factors (TGF-β1 and PDGF) from the fabricated biocomposites with ELISA kit. In this study, Figure 5b shows the amounts of PRP-derived growth factors (TGF-β1 and PDGF) released per measuring day from the biocomposite. The loss of growth factors during the washing/cross-linking/hydrolysis process was about 12−15 ng/mL and the amount of loss was about 10−20% of the accumulated amount until 35 days. The results of the analysis of cumulated release showed that the initial bursts (0−12 h) were well controlled and continuous release was obtained until 35 days. Although the growth factors (PDGF: 27−31 kDa and TGF-β1:25 kDa) were of different sizes,[48,49] the release behavior of the growth factors from the biocomposite was similar, and their release was effectively

DOI: 10.1021/acsbiomaterials.7b00640
ACS Biomater. Sci. Eng. XXXX, XXX, XXX−XXX

deterred by TA, which could have chemically reacted with the collagen and the various growth factors contained in PRP (Figure 5c–e). Figure 5c shows that when 0.1 wt % of TA was mixed with PRP, the reacted particles were observed in the mixing tube. This image showed indirectly protein of PRP chemically cross-linked with TA. The reaction phenomenon is explained in the schematic description of Figure 5d, e. Collagen cross-links with TA using hydrogen bonds and hydrophobic interactions between the carbon atoms of TA and the amino acids (proline residue) of collagen.[50−52] Because the growth factors from the PRP are also proteins,[38,53] we believe that TA could have formed hydrogen bonds or hydrophobic interactions with these components (Figure 5e).

Batycky et al. established theoretical model of drug release from biodegradable scaffolds.[54] They classified release phenomenon with three stages: initial burst, induction time, and continuous release. To evaluate our release profile of TGF-β1 and PDGF, we also classified release curve with three stages. In Figure 5b-A shows the initial burst affected by desorption of growth factors located on the surface and the mesopore connected to the external surface. Continuous release by diffusion after induction time showed in Figure 5b-B. However, it is hard to distinguish the induction time that appeared between the initial burst and continuous release. According to the model of Batycky et al., because of slow desorption or rapid degradation of scaffolds, induction period cannot distinguish.[54] In our release profile of TGF-β1 and PDGF, we cannot distinguish induction period and it indicated that slow desorption or rapid degradation of scaffolds. Considering the degradation rate (Figure 4g), the scaffolds did not show rapid degradation. We can then believe the macromolecular growth factors release with slow desorption by cross-link PRP and collagen with TA.

3.5. In Vitro Cellular Activities. It is well-known that the efficiency of cell seeding can directly influence initial cell adhesion and finally regenerated tissue homogeneity, and it is highly dependent on pore geometry, including porosity and pore interconnectivity, and surface chemical components and physical topography.[26] Figure 6a shows the efficiency of cell seeding on the control (CON) and PRP biocomposites (PRP). As expected, the seeding efficiency on both the scaffolds (control: 40.64 ± 6.40% and PRP biocomposite: 39.28 ± 4.47%) was very similar because the control and PRP biocomposites had similar chemical compositions, pore geometry, and surface roughness.

To observe the cellular response to the scaffolds, we used the control and PRP biocomposites, which had similar pore geometry. First, we performed live (green)/dead (red) cell assays using MC3T3-E1 preosteoblasts to determine cell viability on the biocomposites. The measurement was conducted for several periods (12 h, 1 day, 3 days, 6 days, and 9 days of cell culture). As presented in the Figure 6b, most cells on both the scaffolds were well attached, proliferated, and viable until 9 days of cell culture. In addition, the cell viability for both the scaffolds was similar and high, indicating that the scaffolds were safe biomaterials (Figure 6c).

The PicoGreen assay was conducted to quantitatively observe cell proliferation (Figure 6d). The DNA content on both the scaffolds increased continuously until 9 days. The difference in the DNA content between the control and PRP biocomposites during cell adhesion at initial period was not significantly different. However, during the overall culture for 9 days, the cell proliferation for the PRP biocomposite has been much higher than that of the control biocomposite. These results indicated that continuously released PRP-derived growth factors enhanced the cell proliferation.

Figure 7a shows the nuclei (blue color) and F-actin (red color) of the control and PRP biocomposites at 6, 9, and 12 days of cell

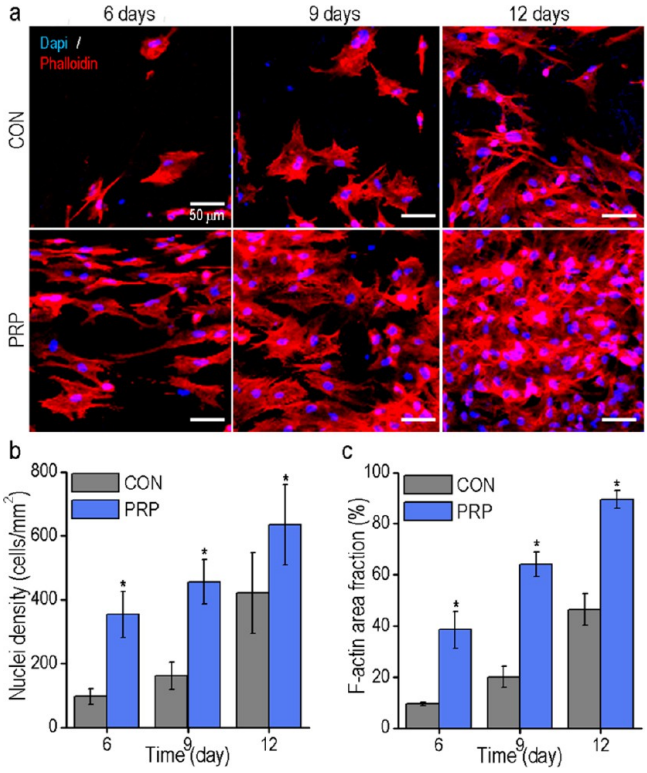

Figure 7. (a) DAPI/Phalloidin images, (b) nuclei density, and (c) F-actin area fraction of the CON and PRP scaffolds at 6, 9, and 12 days. * indicates $p < 0.05$.

culture. As expected based on the results of DNA content analysis and live/dead images, the nuclei and cytoskeleton on the PRP biocomposite were more extensively spread than on the control biocomposite (Figure 7b, c).

ALP activity indicates early stage of osteoblastic differentiation.[55] In Figure 8a, the ALP activities for the control and PRP biocomposites were measured and the values were normalized with the DNA contents. The ALP activities of the preosteoblasts on both scaffolds were expressed much earlier compared to other synthetic or natural scaffolds.[56,57] Similar phenomenon was also previously observed in another study for CDHA prepared by hydrolysis of α-TCP at 37 °C.[58] In that research, preosteoblast cells showed fast maturation and mineralization, which were due to the cell-favorable microenvironment and the stimulation of the intracellular activities without osteogenic supplements.[58] Moreover, the ALP activity without normalization at 3 days of cell culture was significantly higher in the PRP biocomposite than in the control biocomposite. However, considering the normalized data, control group showed higher ALP activity than the PRP group at 1 and 9 days of culture, due to the high cell proliferation rate induced by the release of PRP-derived growth factors, such as PDGF and TGF-β1. It is known that the PDGF stimulates the mitogenesis of stem cells and osteoblasts, which increases cell number, and that TGF-β1 activates preosteoblast to proliferate and mature.[7,38,39,59,60] Based on the results, we carefully expected that the PRP-derived growth factors could accelerate preosteo-

DOI: 10.1021/acsbiomaterials.7b00640
ACS Biomater. Sci. Eng. XXXX, XXX, XXX−XXX

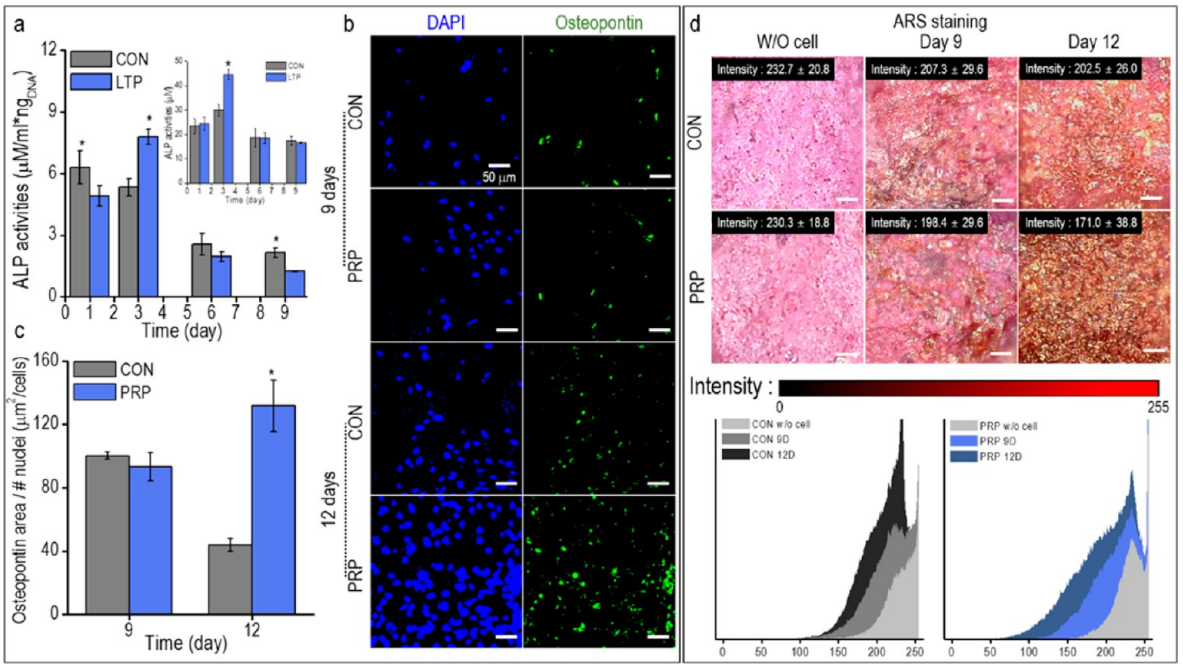

Figure 8. (a) ALP activities of the CON and PRP scaffolds at 1, 3, 6, and 9 days. (b) Fluorescence images of DAPI and osteopontin staining, and (c) osteopontin area analysis at 9 and 12 days. (d) Optical images of Alizarin Red-S (ARS) staining and red color intensity analysis of the captured images of scaffolds without cell, CON, and PRP scaffolds. * indicates $p < 0.05$.

blast cell proliferation and differentiation with calcium phosphate scaffold.

The fluorescence images of osteopontin (OPN) of the control and PRP biocomposites at 9 and 12 days after culture were obtained (Figure 8b), and the OPN area divided by the number of nuclei was measured quantitatively (Figure 8c). The results showed that the PRP group showed higher OPN level at 12 days. The alizarin red-S (ARS) staining of the two groups was performed for both without and with cell culture for 9 and 12 days in Figure 8d. We evaluated the amount of the calcium deposition of the composites by calculating the red color intensity (0−255) in the ARS staining images. Lower red color intensity values (closer to 0) indicate more calcium deposition, because the more the preosteoblast cells differentiated, the more the color of the cells darkened. The scaffolds without cells showed pink color (red color intensity; CON, 232.7 ± 20.8; PRP, 230.3 ± 18.8) due to the calcium in CDHA stained in red color. However, the images of scaffolds with cell culture for 9 and 12 days showed comparatively dark red color because of the calcification of the scaffolds by the preosteoblasts. In addition, the red color intensity of the PRP group is lower than CON group at day 9 (CON: 207.3 ± 29.6, PRP: 198.4 ± 29.6) and day 12 (CON: 202.5 ± 26.0, PRP: 171.0 ± 38.8) of cell culture. In other words, these results indicated that the PRP group has shown higher differentiation and mineralization than the CON group.

Platelet-rich plasma (PRP) contains diverse growth factors such as PDGF, TGF-β1, and IGF, which can promote bone regeneration.[7,38] Nevertheless, the efficacy of PRP for bone regeneration still remains controversial with both in vitro and in vivo tests.[40−42,60−62] In an in vitro test, CDHA and β-TCP scaffolds with PRP showed better proliferation and differentiation of human mesenchymal stem cells (hMSC) than the groups without PRP.[61] Other studies reported that CDHA scaffold with PRP and stem cells enhanced bone regeneration in in vivo rabbit models.[40,42,62] On the other hand, a research group reported that CDHA or β-TCP scaffolds with PRP did not show any enhanced osteogenic properties compared to scaffolds without PRP in mouse model.[41] Anita et al. also reported that there is no significant difference between with or without PRP samples in sheep model for bone repair.[60] In our results, PRP enhanced the proliferation and differentiation of the preosteoblasts with in vitro culture. Further studies will be needed, however, focusing on the confirmation of the effects of PRP with the use of CDHA on bone regeneration in in vivo tests.

4. CONCLUSION

In this study, a ceramic-based biocomposite, consisting of CDHA/collagen mixture and PRP, was manufactured using the low-temperature 3D printing system and postprinting treatment of proper cross-linking and hydrolysis processes. The long-term release of PRP-derived growth factors (PDGF and TGF-β1) from the biocomposite was verified. The growth factors from the biocomposite were continuously released up to 35 days due to the cross-linking by tannic acid. Regardless of the controversy about the efficacy of PRP for bone regeneration, the results of our in vitro test using preosteoblasts showed that the cell proliferation and bone mineralization of the PRP biocomposite scaffold were significantly better than those of the control. The results implied that the continuously released PRP showed positive effects on the preosteoblast cells in terms of the cell proliferation and differentiation. On the basis of these results, our PRP biocomposite has potential for the use as an outstanding bioactive scaffold for bone tissue regeneration.

■ ASSOCIATED CONTENT

Supporting Information

The Supporting Information is available free of charge on the ACS Publications website at DOI: 10.1021/acsbiomaterials.7b00640.

Figure S1 and additional information (PDF)

DOI: 10.1021/acsbiomaterials.7b00640
ACS Biomater. Sci. Eng. XXXX, XXX, XXX−XXX

AUTHOR INFORMATION

Corresponding Author

*E-mail: gkimbme@skku.edu. Tel.: +82-31-290-7828.

ORCID

GeunHyung Kim: 0000-0002-2965-2171

Notes

The authors declare no competing financial interest.

ACKNOWLEDGMENTS

This study was supported by a grant from the Ministry of Trade, Industry & Energy (MOTIE, Korea) under Industrial Technology Innovation Program (10063541: Development of bioceramic 3D printing materials and low temperature (<40 °C) process customized by implant sites) and also supported by a grant from the National Research of Korea grant funded by the Ministry of Education, Science, and Technology (MEST) (Grant NRF-2015R1A2A1A15055305).

ABBREVIATIONS

α-TCP, alpha tricalcium phosphate
CDHA, calcium-deficient hydroxyapatite
TA, tannic acid
PDGF, platelet derived growth factor
IGF, insulin-like growth factors
RTP, room-temperature printing
PBS, phosphate buffer saline
β-TCP, beta tricalcium phosphate
PRP, platelet-rich plasma
CPC, calcium phosphate cement
TGF-β1, transforming growth factor-beta 1
LTP, low-temperature printing
ALP, alkaline phosphatase
BSA, bovine serum albumin

REFERENCES

(1) Amini, A. R.; Laurencin, C. T.; Nukavarapu, S. P. Bone Tissue Engineering: Recent Advances and Challenges. *Crit. Rev. Biomed. Eng.* **2012**, *40*, 363−408.

(2) Younger, E. M.; Chapman, M. W. Morbidity at Bone Graft Donor Sites. *J. Orthop. Trauma* **1989**, *3*, 192−195.

(3) Bose, S.; Tarafder, S. Calcium Phosphate Ceramic Systems in Growth Factor and Drug Delivery for Bone Tissue Engineering: A Review. *Acta Biomater.* **2012**, *8*, 1401−1421.

(4) Tarafder, S.; Nansen, K.; Bose, S. Lovastatin Release from Polycaprolactone Coated β-Tricalcium Phosphate: Effects of pH, Concentration and Drug−Polymer Interactions. *Mater. Sci. Eng., C* **2013**, *33*, 3121−3128.

(5) Sekhon, U. D. S.; Sen Gupta, A. Platelets and Platelet-Inspired Biomaterials Technologies in Wound-Healing Applications. *ACS Biomater. Sci. Eng.* **2017**, DOI: 10.1021/acsbiomaterials.7b00013.

(6) Dolder, J. V. D.; Mooren, R.; Vloon, A. P.; Stoelinga, P. J.; Jansen, J. A. Platelet-Rich Plasma: Quantification of Growth Factor Levels and the Effect on Growth and Differentiation of Rat Bone Marrow Cells. *Tissue Eng.* **2006**, *12*, 3067−3073.

(7) Lu, H. H.; Vo, J. M.; Chin, H. S.; Lin, J.; Cozin, M.; Tsay, R.; Eisig, S.; Landesberg, R. Controlled Delivery of Platelet-Rich Plasma-Derived Growth Factors for Bone Formation. *J. Biomed. Mater. Res., Part A* **2008**, *86*, 1128−1136.

(8) Lin, K.-F.; He, S.; Song, Y.; Wang, C.-M.; Gao, Y.; Li, J.-Q.; Tang, P.; Wang, Z.; Bi, L.; Pei, G.-X. Low-Temperature Additive Manufacturing of Biomimic Three-Dimensional Hydroxyapatite/Collagen Scaffolds for Bone Regeneration. *ACS Appl. Mater. Interfaces* **2016**, *8*, 6905−6916.

(9) Guo, H.; Su, J.; Wei, J.; Kong, H.; Liu, C. Biocompatibility and Osteogenicity of Degradable Ca-Deficient Hydroxyapatite Scaffolds from Calcium Phosphate Cement for Bone Tissue Engineering. *Acta Biomater.* **2009**, *5*, 268−278.

(10) Ratheesh, G.; Venugopal, J. R.; Chinappan, A.; Ezhilarasu, H.; Sadiq, A.; Ramakrishna, S. 3D Fabrication of Polymeric Scaffolds for Regenerative Therapy. *ACS Biomater. Sci. Eng.* **2017**, *3*, 1175.

(11) Carrodeguas, R. G.; De Aza, S. α-Tricalcium Phosphate: Synthesis, Properties and Biomedical Applications. *Acta Biomater.* **2011**, *7*, 3536−3546.

(12) Durucan, C.; Brown, P. α-Tricalcium Phosphate Hydrolysis to Hydroxyapatite at and near Physiological Temperature. *J. Mater. Sci.: Mater. Med.* **2000**, *11*, 365−371.

(13) Liu, T.-Y.; Chen, S.-Y.; Li, J.-H.; Liu, D.-M. Study on Drug Release Behaviour of CDHA/Chitosan Nanocomposites—Effect of CDHA Nanoparticles. *J. Controlled Release* **2006**, *112*, 88−95.

(14) Zhao, J.; Wang, S.; Bao, J.; Sun, X.; Zhang, X.; Zhang, X.; Ye, D.; Wei, J.; Liu, C.; Jiang, X.; et al. Trehalose Maintains Bioactivity and Promotes Sustained Release of BMP-2 from Lyophilized CDHA Scaffolds for Enhanced Osteogenesis *in vitro* and. *PLoS One* **2013**, *8*, e54645.

(15) Gleeson, J.; Plunkett, N.; O'Brien, F. Addition of Hydroxyapatite Improves Stiffness, Interconnectivity and Osteogenic Potential of a Highly Porous Collagen-Based Scaffold for Bone Tissue Regeneration. *Eur. Cell Mater.* **2010**, *20*, 218−230.

(16) Ferreira, A. M.; Gentile, P.; Chiono, V.; Ciardelli, G. Collagen for Bone Tissue Regeneration. *Acta Biomater.* **2012**, *8*, 3191−3200.

(17) Tarafder, S.; Balla, V. K.; Davies, N. M.; Bandyopadhyay, A.; Bose, S. Microwave-Sintered 3D Printed Tricalcium Phosphate Scaffolds for Bone Tissue Engineering. *J. Tissue Eng. Regener. Med.* **2013**, *7*, 631−641.

(18) Sun, Y.; Chen, W.-L.; Lin, S.-J.; Jee, S.-H.; Chen, Y.-F.; Lin, L.-C.; So, P. T.; Dong, C.-Y. Investigating Mechanisms of Collagen Thermal Denaturation by High Resolution Second-Harmonic Generation Imaging. *Biophys. J.* **2006**, *91*, 2620−2625.

(19) Kim, B.-K.; Kim, S.-G.; Kim, S.-Y.; Lim, S.-C.; Kim, Y.-K. A Comparison of Bone Generation Capability in Rabbits Using Tooth Ash and Plaster of Paris with Platelet-Rich Plasma or Fibrin Sealant. *Oral Surg. Oral Med. Oral Pathol. Oral Radiol. Endod.* **2010**, *110*, e8−e14.

(20) Shiga, Y.; Kubota, G.; Orita, S.; Inage, K.; Kamoda, H.; Yamashita, M.; Iseki, T.; Ito, M.; Yamauchi, K.; Eguchi, Y.; et al. Freeze-Dried Human Platelet-Rich Plasma Retains Activation and Growth Factor Expression after an Eight-Week Preservation Period. *Asian Spine J.* **2017**, *11*, 329−336.

(21) Fels, I. G. Hydration and Density of Collagen and Gelatin. *J. Appl. Polym. Sci.* **1964**, *8*, 1813−1824.

(22) Birks, L.; Friedman, H. Particle Size Determination from X-Ray Line Broadening. *J. Appl. Phys.* **1946**, *17*, 687−692.

(23) Müller, A.; Ni, Z.; Hessler, N.; Wesarg, F.; Müller, F. A.; Kralisch, D.; Fischer, D. The Biopolymer Bacterial Nanocellulose as Drug Delivery System: Investigation of Drug Loading and Release Using the Model Protein Albumin. *J. Pharm. Sci.* **2013**, *102*, 579−592.

(24) Carter, D. C.; Ho, J. X. Structure of Serum Albumin. *Adv. Protein Chem.* **1994**, *45*, 153−203.

(25) Liu, T.-Y.; Chen, S.-Y.; Liu, D.-M.; Liou, S.-C. On the Study of BSA-Loaded Calcium-Deficient Hydroxyapatite Nano-Carriers for Controlled Drug Delivery. *J. Controlled Release* **2005**, *107*, 112−121.

(26) Sobral, J. M.; Caridade, S. G.; Sousa, R. A.; Mano, J. F.; Reis, R. L. Three-Dimensional Plotted Scaffolds with Controlled Pore Size Gradients: Effect of Scaffold Geometry on Mechanical Performance and Cell Seeding Efficiency. *Acta Biomater.* **2011**, *7*, 1009−1018.

(27) Park, H.-J.; Yu, S. J.; Yang, K.; Jin, Y.; Cho, A.-N.; Kim, J.; Lee, B.; Yang, H. S.; Im, S. G.; Cho, S.-W. Paper-Based Bioactive Scaffolds for Stem Cell-Mediated Bone Tissue Engineering. *Biomaterials* **2014**, *35*, 9811−9823.

(28) Şahin, E.; Kalyon, D. M. The Rheological Behavior of a Fast-Setting Calcium Phosphate Bone Cement and Its Dependence on Deformation Conditions. *J. Mech. Behav. Biomed.* **2017**, *72*, 252−260.

DOI: 10.1021/acsbiomaterials.7b00640
ACS Biomater. Sci. Eng. XXXX, XXX, XXX−XXX

(29) MIZUHIRA, V.; FUTAESAKU, Y. New Fixation for Biological Membranes Using Tannic Acids. *Acta Histochem. Cytochem.* **1972**, *5*, 233−236.
(30) Raja, N.; Yun, H.-s. A Simultaneous 3D Printing Process for the Fabrication of Bioceramic and Cell-Laden Hydrogel Core/Shell Scaffolds with Potential Application in Bone Tissue Regeneration. *J. Mater. Chem. B* **2016**, *4*, 4707−4716.
(31) Sabree, I.; Gough, J.; Derby, B. Mechanical Properties of Porous Ceramic Scaffolds: Influence of Internal Dimensions. *Ceram. Int.* **2015**, *41*, 8425−8432.
(32) Karageorgiou, V.; Kaplan, D. Porosity of 3D Biomaterial Scaffolds and Osteogenesis. *Biomaterials* **2005**, *26*, 5474−5491.
(33) Liedert, A.; Kaspar, D.; Blakytny, R.; Claes, L.; Ignatius, A. Signal Transduction Pathways Involved in Mechanotransduction in Bone Cells. *Biochem. Biophys. Res. Commun.* **2006**, *349*, 1−5.
(34) Wei, J.; Igarashi, T.; Okumori, N.; Igarashi, T.; Maetani, T.; Liu, B.; Yoshinari, M. Influence of Surface Wettability on Competitive Protein Adsorption and Initial Attachment of Osteoblasts. *Biomed. Mater.* **2009**, *4*, 045002.
(35) Gotterbarm, T.; Richter, W.; Jung, M.; Berardi Vilei, S.; Mainil-Varlet, P.; Yamashita, T.; Breusch, S. J. An *in vivo* Study of a Growth-Factor Enhanced, Cell Free, Two-Layered Collagen−Tricalcium Phosphate in Deep Osteochondral Defects. *Biomaterials* **2006**, *27*, 3387−3395.
(36) Bian, W.; Li, D.; Lian, Q.; Li, X.; Zhang, W.; Wang, K.; Jin, Z. Fabrication of a Bio-Inspired Beta-Tricalcium Phosphate/Collagen Scaffold Based on Ceramic Stereolithography and Gel Casting for Osteochondral Tissue Engineering. *Rapid Prototyp. J.* **2012**, *18*, 68−80.
(37) Inzana, J. A.; Olvera, D.; Fuller, S. M.; Kelly, J. P.; Graeve, O. A.; Schwarz, E. M.; Kates, S. L.; Awad, H. A. 3D Printing of Composite Calcium Phosphate and Collagen Scaffolds for Bone Regeneration. *Biomaterials* **2014**, *35*, 4026−4034.
(38) Marx, R. E.; Carlson, E. R.; Eichstaedt, R. M.; Schimmele, S. R.; Strauss, J. E.; Georgeff, K. R. Platelet-Rich Plasma: Growth Factor Enhancement for Bone Grafts. *Oral Surg. Oral Med. Oral Pathol. Oral Radiol. Endod.* **1998**, *85*, 638−646.
(39) Dimitriou, R.; Tsiridis, E.; Giannoudis, P. V. Current Concepts of Molecular Aspects of Bone Healing. *Injury* **2005**, *36*, 1392−1404.
(40) Kasten, P.; Vogel, J.; Geiger, F.; Niemeyer, P.; Luginbühl, R.; Szalay, K. The Effect of Platelet-Rich Plasma on Healing in Critical-Size Long-Bone Defects. *Biomaterials* **2008**, *29*, 3983−3992.
(41) Kasten, P.; Vogel, J.; Luginbühl, R.; Niemeyer, P.; Weiss, S.; Schneider, S.; Kramer, M.; Leo, A.; Richter, W. Influence of Platelet-Rich Plasma on Osteogenic Differentiation of Mesenchymal Stem Cells and Ectopic Bone Formation in Calcium Phosphate Ceramics. *Cells Tissues Organs* **2006**, *183*, 68−79.
(42) Kasten, P.; Beverungen, M.; Lorenz, H.; Wieland, J.; Fehr, M.; Geiger, F. Comparison of Platelet-Rich Plasma and VEGF-Transfected Mesenchymal Stem Cells on Vascularization and Bone Formation in a Critical-Size Bone Defect. *Cells Tissues Organs* **2012**, *196*, 523−533.
(43) Fufa, D.; Shealy, B.; Jacobson, M.; Kevy, S.; Murray, M. M. Activation of Platelet-Rich Plasma Using Soluble Type I Collagen. *J. Oral. Maxil. Surg.* **2008**, *66*, 684−690.
(44) Hokugo, A.; Sawada, Y.; Hokugo, R.; Iwamura, H.; Kobuchi, M.; Kambara, T.; Morita, S.; Tabata, Y. Controlled Release of Platelet Growth Factors Enhances Bone Regeneration at Rabbit Calvaria. *Oral Surg. Oral Med. Oral Pathol. Oral Radiol. Endod.* **2007**, *104*, 44−48.
(45) Van Buren, J. P.; Robinson, W. B. Formation of Complexes between Protein and Tannic Acid. *J. Agric. Food Chem.* **1969**, *17*, 772−777.
(46) Yeo, M. G.; Kim, G. H. A Cell-Printing Approach for Obtaining hASC-Laden Scaffolds by Using a Collagen/Polyphenol Bioink. *Biofabrication* **2017**, *9*, 025004.
(47) Cao, N.; Fu, Y.; He, J. Mechanical Properties of Gelatin Films Cross-Linked, Respectively, by Ferulic Acid and Tannin Acid. *Food Hydrocolloids* **2007**, *21*, 575−584.
(48) Raines, E. W.; Ross, R. Platelet-Derived Growth Factor. I. High Yield Purification and Evidence for Multiple Forms. *J. Biol. Chem.* **1982**, *257*, 5154−5160.
(49) Assoian, R.; Komoriya, A.; Meyers, C. A.; Miller, D. M.; Sporn, M. B. Transforming Growth Factor-Beta in Human Platelets. Identification of a Major Storage Site, Purification, and Characterization. *J. Biol. Chem.* **1983**, *258*, 7155−7160.
(50) Velmurugan, P.; Singam, E. R. A.; Jonnalagadda, R. R.; Subramanian, V. Investigation on Interaction of Tannic Acid with Type I Collagen and Its Effect on Thermal, Enzymatic, and Conformational Stability for Tissue Engineering Applications. *Biopolymers* **2014**, *101*, 471−483.
(51) Tscherch, K.; Biller, J.; Lehmann, M.; Trusch, M.; Rohn, S. One- and Two-Dimensional High-Performance Thin-Layer Chromatography as an Alternative Analytical Tool for Investigating Polyphenol−Protein Interactions. *Phytochem. Anal.* **2013**, *24*, 436−445.
(52) Lu, Y.; Bennick, A. Interaction of Tannin with Human Salivary Proline-Rich Proteins. *Arch. Oral Biol.* **1998**, *43*, 717−728.
(53) Phillips, D. R.; Agin, P. P. Platelet Plasma Membrane Glycoproteins. Evidence for the Presence of Nonequivalent Disulfide Bonds Using Nonreduced-Reduced Two-Dimensional Gel Electrophoresis. *J. Biol. Chem.* **1977**, *252*, 2121−2126.
(54) Batycky, R. P.; Hanes, J.; Langer, R.; Edwards, D. A. A Theoretical Model of Erosion and Macromolecular Drug Release from Biodegrading Microspheres. *J. Pharm. Sci.* **1997**, *86*, 1464−1477.
(55) Lian, J. B.; Stein, G. S. Concepts of Osteoblast Growth and Differentiation: Basis for Modulation of Bone Cell Development and Tissue Formation. *Crit. Rev. Oral Biol. Med.* **1992**, *3*, 269−305.
(56) Chou, Y. F.; Dunn, J. C.; Wu, B. M. *In vitro* Response of MC3T3-E1 Preosteoblasts within Three-Dimensional Apatite-Coated PLGA Scaffolds. *J. Biomed. Mater. Res., Part B* **2005**, *75*, 81−90.
(57) Beck, G. R.; Sullivan, E. C.; Moran, E.; Zerler, B. Relationship between Alkaline Phosphatase Levels, Osteopontin Expression, and Mineralization in Differentiating MC3T3-E1 Osteoblasts. *J. Cell. Biochem.* **1998**, *68*, 269−280.
(58) Sethuraman, S.; Nair, L. S.; El-Amin, S.; Nguyen, M. T. N.; Greish, Y. E.; Bender, J. D.; Brown, P. W.; Allcock, H. R.; Laurencin, C. T. Novel Low Temperature Setting Nanocrystalline Calcium Phosphate Cements for Bone Repair: Osteoblast Cellular Response and Gene Expression Studies. *J. Biomed. Mater. Res., Part A* **2007**, *82*, 884−891.
(59) Blom, E.; Klein-Nulend, J.; Klein, C.; Kurashina, K.; Van Waas, M.; Burger, E. Transforming Growth Factor-β1 Incorporated During Setting in Calcium Phosphate Cement Stimulates Bone Cell Differentiation. *J. Biomed. Mater. Res.* **2000**, *50*, 67−74.
(60) Sarkar, M. R.; Augat, P.; Shefelbine, S. J.; Schorlemmer, S.; Huber-Lang, M.; Claes, L.; Kinzl, L.; Ignatius, A. Bone Formation in a Long Bone Defect Model Using a Platelet-Rich Plasma-Loaded Collagen Scaffold. *Biomaterials* **2006**, *27*, 1817−1823.
(61) Kasten, P.; Vogel, J.; Beyen, I.; Weiss, S.; Niemeyer, P.; Leo, A.; Lüginbuhl, R. Effect of Platelet-Rich Plasma on the *in vitro* Proliferation and Osteogenic Differentiation of Human Mesenchymal Stem Cells on Distinct Calcium Phosphate Scaffolds: The Specific Surface Area Makes a Difference. *J. Biomater. Appl.* **2008**, *23*, 169−188.
(62) El Backly, R. M.; Zaky, S. H.; Canciani, B.; Saad, M. M.; Eweida, A. M.; Brun, F.; Tromba, G.; Komlev, V. S.; Mastrogiacomo, M.; Marei, M. K.; Cancedda, R. Platelet Rich Plasma Enhances Osteoconductive Properties of a Hydroxyapatite-β-Tricalcium Phosphate Scaffold (Skelite) for Late Healing of Critical Size Rabbit Calvarial Defects. *J. Cranio. Maxill. Surg.* **2014**, *42*, e70−e79.

DOI: 10.1021/acsbiomaterials.7b00640
ACS Biomater. Sci. Eng. XXXX, XXX, XXX−XXX